Effect of PANI and PPy on electrochemical performance of rGO/ZnMn2O4 aerogels as electrodes for supercapacitors

Effect of PANI and PPy on Electrochemical Performance of rGO/ZnMn2O4 Aerogels as Electrodes for Supercapacitors

LE QUOC BAO,[1,6] ELIF VARGUN,[2,3,7] HAOJIE FEI,[2,8] QILIN CHENG,[2,4,9] CONSTANTIN BUBULINCA,[2,10] ROBERT MOUCKA,[2,11] IRINA SAPURINA,[2,12] TRAN TRONG DAO,[5,13] NATALIA E. KAZANTSEVA[2,14] and PETR SAHA[2,15]

1.—Faculty of Applied Sciences, Ton Duc Thang University, Ho Chi Minh City, Vietnam. 2.—Centre of Polymer Systems, Tomas Bata University in Zlín, Tr. T. Bati 5678, 760 01 Zlín, Czech Republic. 3.—Department of Chemistry, Mugla Sitki Kocman University, 48000 Kotekli, Mugla, Turkey. 4.—Key Laboratory for Ultrafine Materials of Ministry of Education, School of Materials Science and Engineering, East China University of Science and Technology, Shanghai 200237, China. 5.—Division of Modeling Evolutionary Algorithms Simulation and Artificial Intelligence, Faculty of Electrical and Electronics Engineering, Ton Duc Thang University, Ho Chi Minh City, Vietnam. 6.—e-mail: lequocbao@tdtu.edu.vn. 7.—e-mail: elifvargun@gmail.com. 8.—e-mail: haojie@utb.cz. 9.—e-mail: chengql@ecust.edu.cn. 10.—e-mail: bubulinca@utb.cz. 11.—e-mail: moucka@utb.cz. 12.—e-mail: sapurina@utb.cz. 13.—e-mail: trantrongdao@tdtu.edu.vn. 14.—e-mail: kazantseva@utb.cz. 15.—e-mail: saha@utb.cz

Conductive polymers, such as polyaniline (PANI) and polypyrrole (PPy), are widely used in the design of supercapacitors because of their high pseudocapacitive performance as well as facile synthesis and low cost. In this study, hybrid aerogels based on reduced graphene oxide and ZnMn2O4 were modified by PANI and PPy. The 3D structure of the hybrid aerogels was obtained by using a one-step hydrothermal co-assembly method. Then, aniline and pyrrole were polymerized on and within the structure of the hybrid aerogel through in situ polymerization. The electrochemical properties of the hybrid aerogels were studied via cyclic voltammetry and galvanostatic charge-discharge testing to identify the effects of conductive polymers on the electrochemical properties of materials. It has been established that PANI and PPy facilitate an increase of the specific capacitance of rGO/ZnMn2O4 aerogels up to 297.8 F/ g and 108.24 F/g at 0.2 A/g scan rate, respectively.

Key words: Supercapacitor, ternary metal oxide, conductive polymer, hybrid material, aerogel structure

INTRODUCTION

The surge in many human activities in the twenty-first century has created an unprecedented demand for power systems. As a consequence, alternative energy resources utilizing solar, wind, or nuclear energy have been developed. Thus, the requirement for efficient energy storage has become vital. Interest has been focused on supercapacitors (SCs), which have a wide application range, especially in cases of the power boost or energy recovery in automobiles. SCs have a high power density, long life-cycle, and an efficient duration of the charge-discharge process.[1,2]

Being one of the key elements for green energy production in future, graphene derivatives such as graphene/graphene oxide (GO)/reduced graphene oxide (rGO) which have high conductivity and high specific surface areas are important in SCs applications. rGO, in particular, is often used instead of GO because it can provide good dispersion stability and prevent aggregation in the reaction dispersion. Furthermore, the surface architecture of GO/rGO can be used in three-dimensional (3D) carbon

network fabrication for electrode materials.[3-5] Contrary to the two-dimensional (2D) structure of the carbon-based electrode, such as multiwall carbon nanotubes, the 3D porous structures of GO/rGO can exhibit high specific surface areas together with fast mass and electron transport owing to their porous structures.[6,7]

In this study, a hybrid material based on the rGO aerogel was made via the hydrothermal method using the ternary metal oxide of $ZnMn_2O_4$ as a spacing material for SC applications. Transition metal oxide materials, owing to their potential power, energy density, and capacity, have been used in the applications of SC. There are many publications related to the research on the coupling of two semiconductor metal oxides to form a ternary metal oxide which can enhance the specific capacitance and electrochemical performance of SCs.[8-16] Among various kinds of ternary metal oxides, $ZnMn_2O_4$ appears to have great potential due to its advantages in magnetic, photocatalytic, and electrochemical performance.[17] In 2018, the application of carbon-coated ZnMn2O4 nanocrystallite SCs that exhibited the specific capacitance of 150 F/ g in Na_2SO_4 electrolyte was reported by Abdollahi-far et al.[18] This study illustrated that the combination of ternary metal oxides and carbon-based materials could exhibit good electrochemical performance when used as the electrode for a SC.[12,19,20]

The 3D porous hybrid nanostructure provides enough free space to accommodate conductive polymers, the polyaniline (PANI) and/or polypyrrole (PPy). Hence, the loading of PANI and PPy into the hybrid aerogels not only increases the conductivity of the electrodes but also facilitates the electrochemical performance of the SC. In energy storage applications, PANI and PPy have advantages, such as good electrical conductivity, high charge densities, low cost, and excellent pseudocapacitive performances. They have been utilized to improve the device through taking part in a redox reaction, which stores charge.[21-24] The hybrid aerogel structures were fabricated via a one-step co-assembly method and the conductive polymer was deposited onto the structure via an in situ chemical polymerization reaction. The electrochemical properties of the obtained materials were assessed to determine their potential for use as electrode material in an SC.

EXPERIMENTAL

Materials

Natural graphite powder (< 20 am), manganese (II) chloride tetrahydrate ($MnCl_2{\cdot}4H_2O$), zinc acetate dihydrate ($Zn(CH_3COO)_2{\cdot}2H_2O$), potassium permanganate (KMnO4), ammonium sulfate ($(NH_4)_2SO_4$), aniline, pyrrole, and urea are all products of Sigma-Aldrich. Sulfuric acid (96%), perchloric acid ($HClO_4$, 70%), hydrogen peroxide solution (30%), manganese (II) chloride tetrahy-drate ($MnCl_2{\cdot}4H_2O$), and all solvents were purchased from local companies such as PENTA and VWR Chemicals. All the chemicals were used without any further purification.

Synthesis of $ZnMn_2O_4$

$ZnMn_2O_4$ nanoparticles were prepared via a temperature-controlled hydrothermal method. First, $Zn(CH_3COO)_2{\cdot}2H_2O$ (4.39 g, 0.02 mol) and $MnCl_2{\cdot}4H_2O$ (7.92 g, 0.04 mol) were dissolved in 50 mL deionized (DI) water and continuously stirred for 30 min. Urea (1.2 g, 0.02 mol) was then added to the solution. Next, the solution was stirred for 30 min before being sonicated for another 30 min. All the components were entirely dissolved in the solution. Afterward, the solution was transferred to a teflonated autoclave and kept at 180°C for 12 h in an oven. The autoclave was cooled to room temperature after the reaction time. The product that had precipitated in the autoclave was filtered

and washed several times with DI water and acetone before being dried at 70°C for 24 h. The final product of $ZnMn_2O_4$ (3.10 g) was received after being calcinated at 600°C for 5 h.

Preparation of GO

Graphene oxide was prepared according to Hummers' method. First, 3 g of graphite flakes were put into a 4-neck-flask in an ice bath. Then, 75 mL of H_2SO_4 (96%) was slowly added to the flask, and stirred for 1 h before 9 g of $KMnO_4$ was slowly added to the mixture. The mixture was then stirred for 3 h before 100 mL of DI water was added to it dropwise. Next, 150 mL of DI water was also added to the mixture. Finally, 20 mL of hydrogen peroxide (30%) was slowly added to the mixture followed by stirring for 30 min in the ice bath. Subsequently, the mixture was washed with DI water and centrifuged many times until its pH was approximately neutral. The GO was then freeze-dried and kept in cold conditions for further experiments.

Synthesis of rGO/$ZnMn_2O_4$

rGO/$ZnMn_2O_4$ aerogel was synthesized using a one-step hydrothermal co-assembly method. First, $ZnMn_2O_4$ was dispersed into a GO suspension (40 mg/mL) in DI water with a ratio of 1:3. The mixture was sonicated for 60 min, and then the content was transferred into an autoclave, which was then heated to 160°C and kept at that temperature for 5 h before being cooled to room temperature. The hybrid hydrogel was collected and washed several times with DI water and kept in 10 mL of DI water.

In Situ Polymerization of Aniline and Pyrrole on and within the rGO/$ZnMn_2O_4$ (rGO/ $ZnMn_2O_4$@PANI, rGO/$ZnMn_2O_4$@PPy).

The hybrid aerogel of rGO/$ZnMn_2O_4$ was cut into pieces and modified with aniline and pyrrole according to the published polymerization process.[25] The piece of graphene hydrogel was immersed in 50 mL of DI water in a 100-mL beaker, then 1.5 mL of monomer (aniline or pyrrole) was added. The beaker was then covered and kept at room temperature for 2 h. This step was repeated before the piece of aerogel was immersed in 50 mL of a solution of perchloric acid (6.8%) and kept there for 18 h. The solution was then removed, and the piece of aerogel was immersed in an aqueous solution of perchloric acid (9.2%, 22 mL) and kept at 0°C for 1 h. Next, an aqueous solution of ammonium persulfate (17.5 mM, 10 mL) was added dropwise to the solution of perchloric acid while this was being stirred. The piece was then kept in the solution at 0°C for 24 h in order to polymerize. Finally, it was washed several times with DI water and then freeze-dried.

Characterization of Aerogels

The crystal structure of the $ZnMn_2O_4$ was analyzed with the help of x-ray diffraction techniques (XRD; Advance D8, Bruker) with Cu-Ka radiation, 0.1540560 nm wavelength and a current of about 1 iA. The chemical composition of rGO/$ZnMn_2O_4$@-pAnI and rGO/$ZnMn_2O_4$@PPy were identified by ATR-FTIR spectroscopy using a Nicolet iS10 (Thermo Scientific) equipped with an ATR sampling accessory with a Ge. The pore morphologies were characterized by a NANOSEM 450 (FEI, USA) scanning electron microscope (SEM) operated at 5 kV under 90 Pa pressure.

Fabrication of Working Electrode and Electrochemical Test

The electrochemical test was performed by making a slurry of crushed aerogel powder with a solution of PTFE (10% of total mass) in 1 mL EtOH. The slurry was coated in the shape of a circle of 0.25 cm radius onto a titanium mesh and then compressed. The electrochemical performance of the as-prepared electrodes was characterized by cyclic voltammetry (CV), galvanostatic charge-discharge tests, and electrochemical impedance spectroscopy (EIS) techniques, using a potentiostat Autolab PGSTAT-128 N at room temperature. Electrochemical measurements were performed in a three-electrode cell using Pt clips as a current collector for the working electrodes. Platinum wire with a large specific area and an Ag/AgCl electrode were used as the counter and reference electrodes, respectively. Measurements were carried out in an aqueous solution of two different electrolytes, 1 M H_2SO_4 and 1 M Na_2SO_4, at room temperature.

EIS measurements were conducted on aerogel structure-coated electrodes in constant voltage mode (0.02 V vs. Ag/AgCl) by sweeping frequencies from 100 kHz to 0.01 Hz at an amplitude of 0.01 VRMS.

The cycling stability of the prepared materials was measured in a two-electrode system using BioLogic battery cyclers (BCS-810) at the current density of 1 A/g for 5000 times. In the two-electrode system, two identical electrodes were compressed in a Swagelok cell and separated by a piece of supercapacitor separator (NKK-MPF30AC).

RESULTS AND DISCUSSION

It has been reported that rGO exhibits good electrical conductivity, high surface area compared to volume ratio, short diffusion distance, and thermal and chemical stability. However, the structure of this material consists of various graphene sheets that can be re-stacked due to van der Waals interactions between adjacent sheets. The re-stacking phenomenon can lead to irreversible capacity loss and reduced surface area. The aerogel made of graphene oxide and $ZnMn_2O_4$ nanoparticles was fabricated to surpass the issues of rGO. $ZnMn_2O_4$ used as the spacer in the aerogel structure can prevent the agglomeration and re-stacking of rGO sheets while increasing the surface area.[8-12] Owing to their flexibility, high conductivity, and simple synthetic process, PANI and PPy are used to improve the working performance of SCs. It has been reported that PANI or PPy have been synthesized separately and used as components to make the hybrid aerogel with rGO.[6,26-28] In this study, PANI and PPy were synthesized inside the structure of the prepared aerogel via the in situ chemical polymerization process. The effect of PANI and PPy on the working performance of the SC electrode was investigated by CV, galvanostatic charge-discharge tests, and EIS analysis.

GO was reduced to rGO which resulted in a clean and transparent solution.

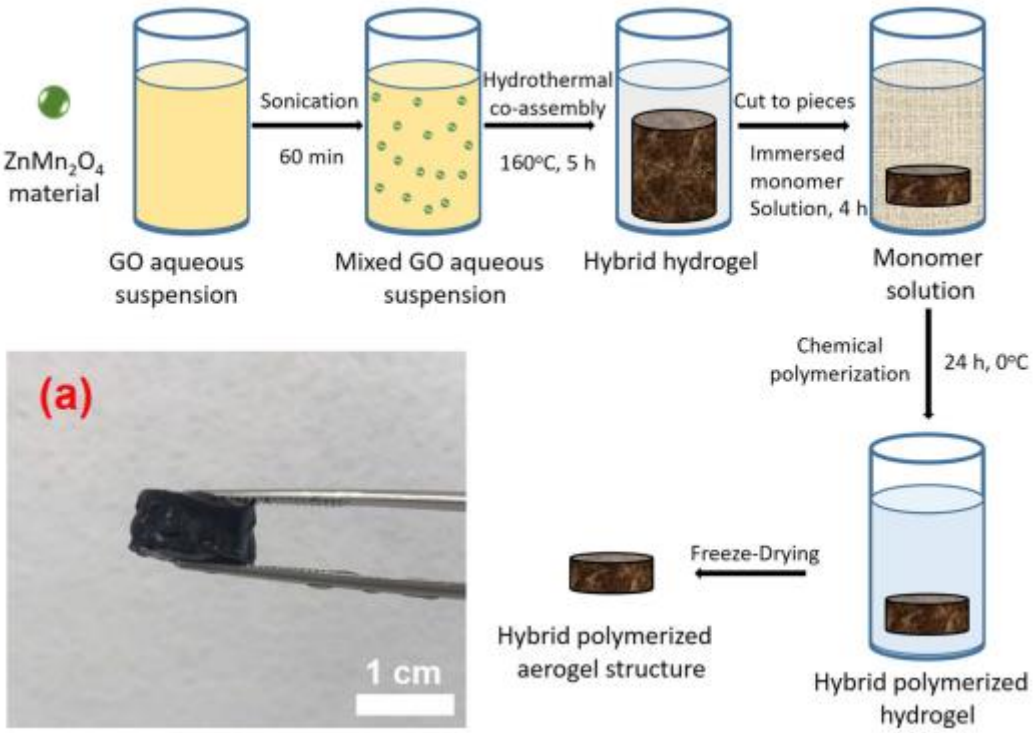

Fig. 1. Schematic of the preparation process of the hybrid aerogel based on rGO, $ZnMn_2O_4$ and conducting polymers (PANI, PPY). (a) Hybrid hydrogel.

Morpho-Structural Properties

The integrated hybrid aerogel is shown in **Fig. 2a.** In the aerogel composite, $ZnMn_2O_4$ played a role as a spacing agent, which could help to prevent the aggregation of the graphene sheets. The hybrid aerogel was modified with PANI and PPy following by freeze-drying to obtain the final materials, which were characterized by SEM to determine their morphology (**Fig. 2**). rGO/$ZnMn_2O_4$ exhibited a well-defined 3D microstructure network of rGO sheets together with small aggregates of ZnMn2O4 nanoparticles randomly distributed in the aerogel (**Fig. 2a**). As seen in **Fig. 2b**, PANI covered the rGO sheets. However, in the case of an aerogel with PPy, the polymerization took place on the rGO sheets and also formed precipitates in the formed of aggregates (**Fig. 2c**).

The XRD pattern of $ZnMn_2O_4$ is shown in **Fig. 3a**, displaying high-intensity diffraction peaks assigned to a crystalline structure. The peak positions at 29.38°, 33.63°, 37.5°, 59.63°, 61.8°, and 65.12° correspond to the crystalline planes of (112), (103), (211), (321), (224) and (400), respectively. The diffraction planes have been identified as a body-centered tetragonal structure of $ZnMn_2O_4$.[19]

FTIR spectra of graphene oxide aerogels supported with PANI and PPy are depicted in **Fig. 3b**. Graphene flakes after oxidation will contain oxygen-groups on their structures. The peaks observed at

3420-3500 cm^{-1} and 1620 cm^{-1} correspond to OH stretching and OH deformation vibrations of the hydroxyl group of graphene oxide. In all the spectra, the peaks at 2980 cm^{-1} and 2890 cm^{-1} show the symmetric and asymmetric stretching vibrations of CH2 molecules, respectively, of rGO aerogels. Peaks at 1737 cm^{-1} represent the C=O stretching vibration of sp^2 carbon due to the carboxylic group site at the edge of the GO. The presence of peaks at 1099 cm^{-1} and 1216 cm^{-1} are due to C-O stretching vibrations and the carbonyl group leftover during reduction. The presence of $ZnMn_2O_4$ was confirmed

by the peaks of 692 cm^{-} attributed to the M-O bond vibrations (M = Zn, Mn). FTIR spectra of rGO/ $ZnMn_2O_4$@PANI revealed peaks at 1210 cm^{-1} and 1232 cm^{-1} which correspond to the aliphatic C-N stretching vibration. rGO/$ZnMn_2O_4$@PPy spectra revealed peaks at 1223 and 1219, which represent the appearance of aromatic C-N stretching. The broad peak at 1592 cm^{-1} was assigned to the C=C stretching vibration of the carbon ring. However, it can also be seen as the C=C stretching vibration of the quinoid and benzenoid rings of PANI or C-C, C-N stretching vibration in PPy.[6,19] The characteristic peaks of the XRD patterns and FT-IR spectra of aerogels confirmed the successful formation of the aerogels based on GO, $ZnMn_2O_4$, PANI, and PPy.

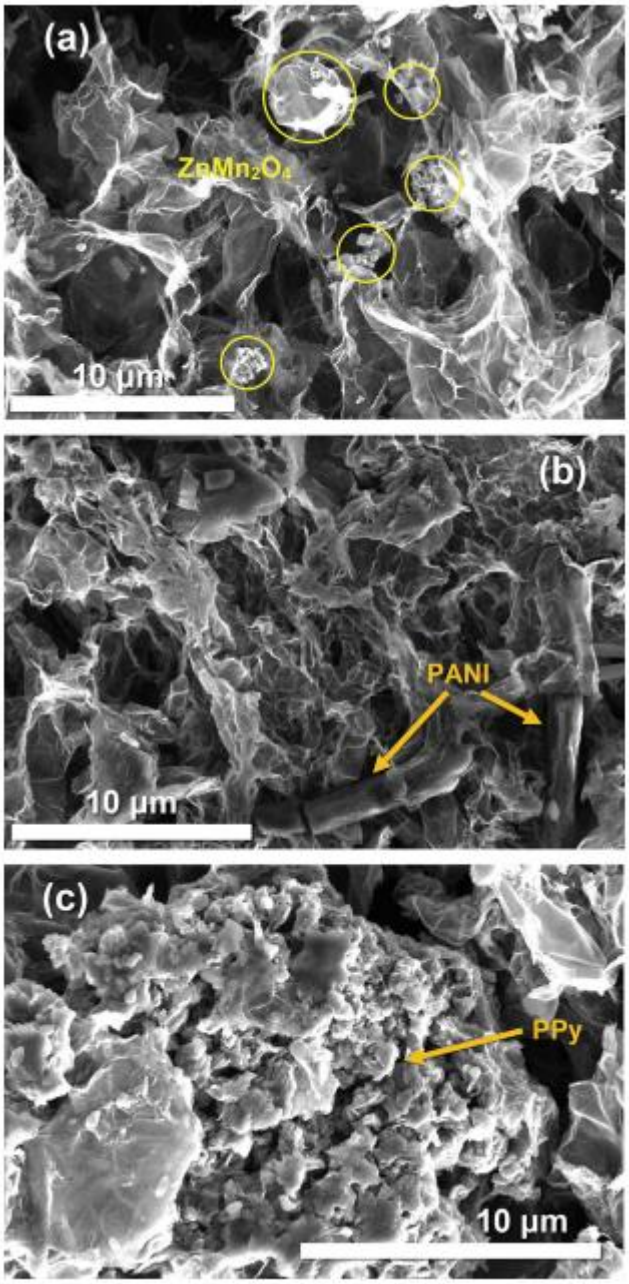

Fig. 2. SEM images of (a) rGO/$ZnMn_2O_4$, (b) rGO/$ZnMn_2O_4$@PANI, and (c) rGO/$ZnMn_2O_4$@PPy.

Cyclic Voltammetry (CV) Analysis

CV measurements were carried out to evaluate the redox reactions of the SC devices. Usually, sulfuric acid (H_2SO_4) is used as an aqueous acid electrolyte in SC due to its high conductivity. When H_2SO_4 was used as the electrolyte, not only carbon-based SC exhibited good specific capacitance, but also their composites with PANI and graphene exhibited high electrochemical performance.[29-31] However, when the graphene is modified with PPy, a more suitable electrolyte for such system was reported by Cai et al.[32] It was found that for the graphene-PPy composite the use of a neutral aqueous electrolyte based on sodium sulfate (Na_2SO_4) provided the best capacitive behavior of the SC.[32] Therefore, when the aerogels were modified with PANI and PPy, the CV analysis of the samples was carried out in two different aqueous electrolytes.

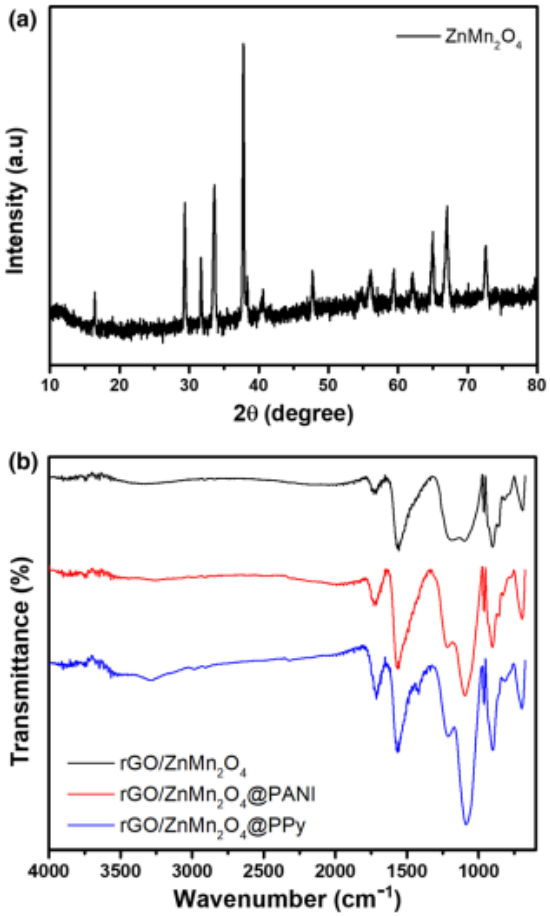

Fig. 3. (a) Powder x-ray diffraction pattern of $ZnMn_2O_4$, and(b) FTIR spectra of rGO/$ZnMn_2O_4$, rGO/$ZnMn_2O_4$@PANI, and rGO/ $ZnMn_2O_4$@PPy.

Effect of PANI and PPy on Electrochemical Perfomace of rGO/ZnMn2O4 Aerogels as Electrodes for Supercapacitors rGO/ZnMn2O4@PANI and rGO/ZnMn2O4@PPy were tested in 1 M H2SO4 and 1 M Na2SO4, respectively. The rGO/ZnMn2O4 hybrid structure was also tested in the same electrolytes under the same conditions as rGO/ZnMn2O4@PANI and rGO/ $ZnMn_2O_4$@PPy, in order to compare their performance. The CV was measured at different scan rates from 5 mV/s to 100 mV/s in a fixed potential window of — 0.2 V to 0.8 V, as illustrated in **Figs. 4 and 5.** In these, small redox peaks can be seen at the potential range of 0.4-0.5 V, implying the contribution of the pseudo-characteristic of metal oxide. This is mainly due to the contribution enhanced by the redox reaction of Zn_2MnO_4. The possible reactions of $ZnMn_2O_4$ might be expressed by the following equations:

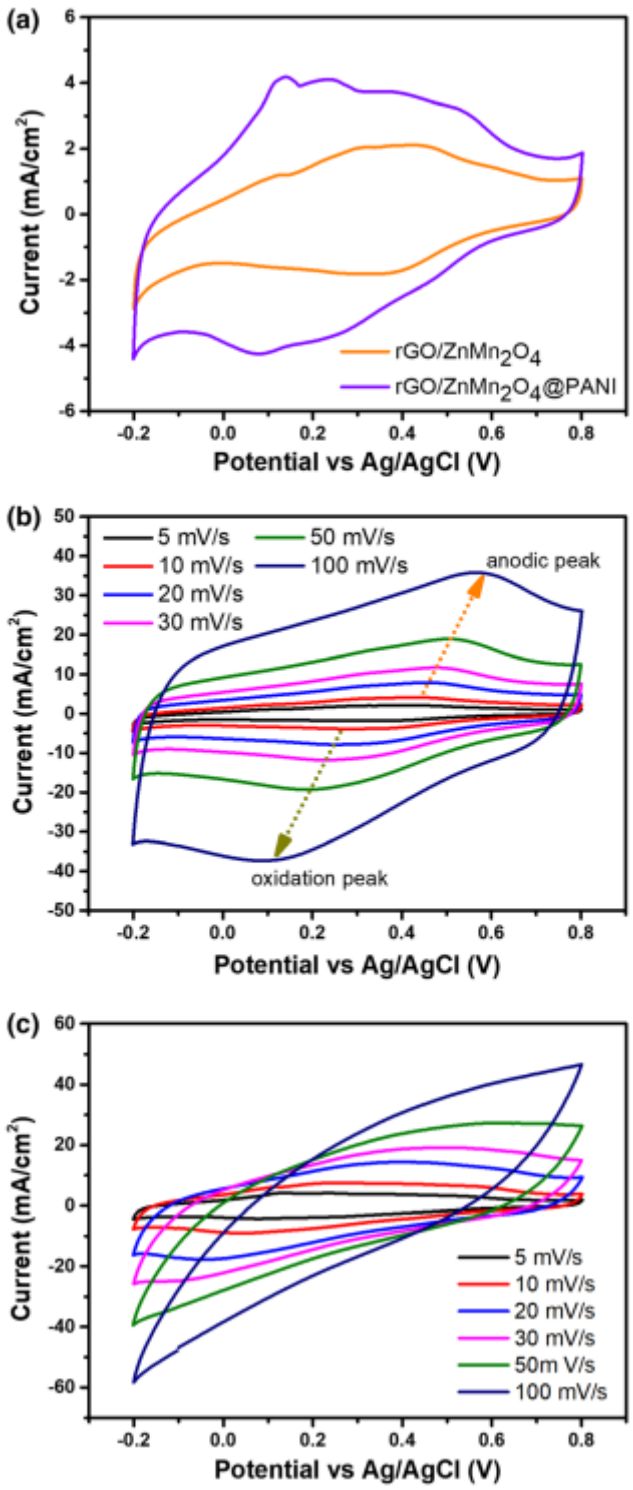

Fig. 4. Cyclic voltammetry of (a) rGO/$ZnMn_2O_4$ and rGO/ $ZnMn_2O_4$@PANI at 5 mV/s, (b) rGO/$ZnMn_2O_4$, and (c) rGO/ $ZnMn_2O_4$@PANI in H_2SO_4.

The possible reactions of $ZnMn_2O_4$ might be expressed by the following equations:

$$(\mathrm{ZnMn_2O_4})_{\mathrm{surface}} + \mathrm{M}^{+} + e^{-} \leftrightarrow [\mathrm{MZnMn_2O_4}]_{\mathrm{surface}} \quad (1)$$

$$ZnMn_2O_4 + M^+ + e^- \leftrightarrow [ZnMn_2O_4]M \qquad (2)$$

where M^+ resembled H^+ (in H_2SO_4) and Na^+ (in Na_2SO_4). The intercalation of M^+ during reduction and de-intercalation upon oxidation may happen in the voids of $ZnMn_2O_4$, resulting in redox reactions.[33]

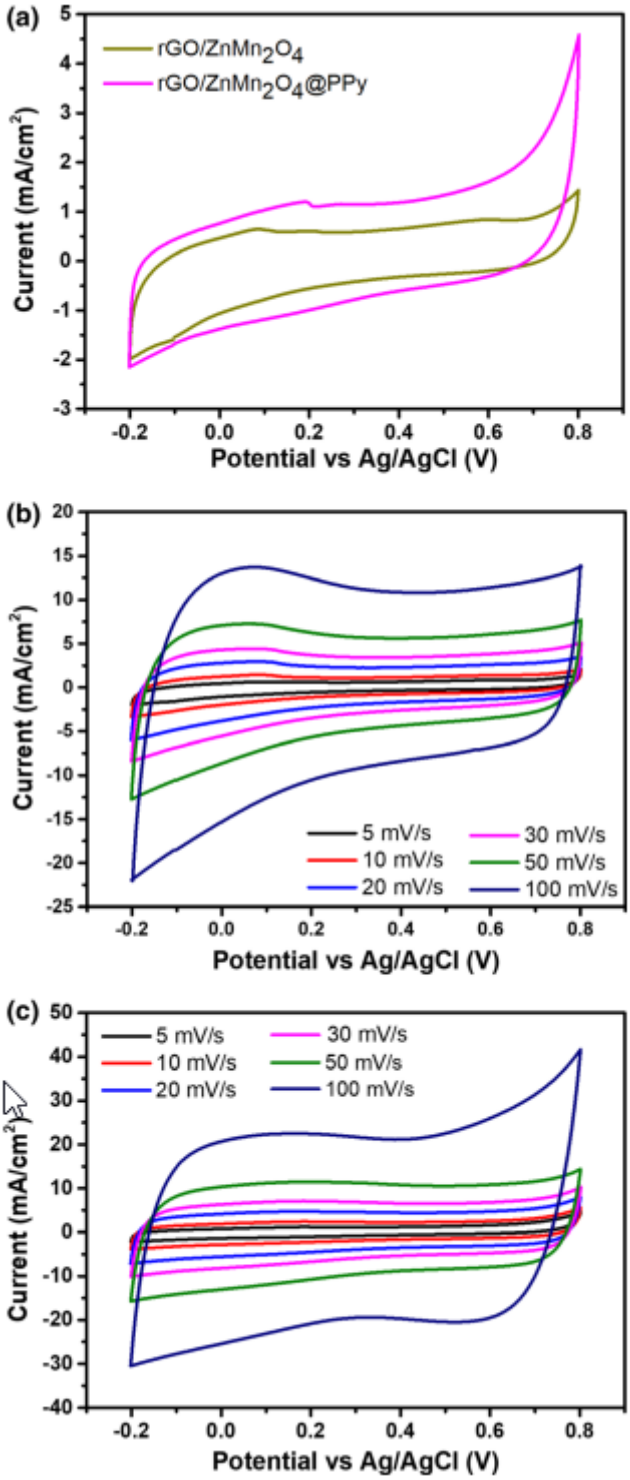

Fig. 5. Cyclic voltammetry of (a) rGO/$ZnMn_2O_4$ and rGO/ $ZnMn_2O_4$@PPy at 5 mV/s, (b) rGO/$ZnMn_2O_4$, and (c) rGO/ $ZnMn_2O_4$@PPy in Na_2SO_4.

The typical CV of the composite rGO/ $ZnMn_2O_4$, rGO/$ZnMn_2O_4$@PANI, and rGO/ $ZnMn_2O_4$@PPy used as electrodes can be attributed to one side of the change in oxidation states of PANI/PPy and on the other side to the oxidative processes of Mn^{2+} and Zn^0 to Mn^{3+} and Zn^{2+}, and to the reduction of Mn^{3+} to Mn^{2+} and Zn^{2+} to Zn^0, respectively (**Figs. 4a and 5a**).[34]

In the CV spectra shown in **Fig. 4a** and b, the cathodic and anodic peaks indicate that the redox process occurred at all scan rates of rGO/$ZnMn_2O_4$ in the electrolyte. The hybrid aerogel structure of both rGO/$ZnMn_2O_4$ and rGO/$ZnMn_2O_4$@PANI showed rectangular peaks with the presence of redox peaks, which confirmed that there was a contribution of EDLC and a pseudocapacitance effect.[27,35] As appears in **Fig. 4b**, the curves of the CV spectra of rGO/$ZnMn_2O_4$ at different scan rates were not symmetric. With increasing scan rates, the oxidation peaks shifted slightly to the left while the anodic peaks moved slightly to the right. The shifts of the peaks' potential were caused by the mechanism of electric polarization, which will cause an irreversible reaction at very high sweep rates.[19] The current response in the rGO/$ZnMn_2O_4$@PANI at the 5-mV/s scan rate was higher than rGO/$ZnMn_2O_4$, which can be attributed to the incorporation of PANI in the structure of the hybrid aerogel. The introduction of PANI to the composite structure of the aerogel can improve the ion diffusion rate and lead to efficient electron transport between the electrode and the electrolyte.[36,37] The CV spectra at different scan rates of GA/$ZnMn_2O_4$@PANI demonstrated the enhancement of the electrochemical performance due to the PANI introduction to the structure (**Fig. 4c**). The specific capacitance of the samples was related to its CV curve area. When the CV curve areas increased, the specific capacitance was enhanced proportionally. From the CV spectra, it thus follows that the specific capacity of rGO/$ZnMn_2O_4$ @ PANI is higher than the specific capacity of rGO/$ZnMn_2O_4$.[37]

The CVs spectra of the hybrid aerogel materials of rGO/$ZnMn_2O_4$ and rGO/$ZnMn_2O_4$@PPy tested in 1 M Na_2SO_4 are shown in **Fig. 5**. With increasing scan rates, the CV curves of rGO/$ZnMn_2O_4$ and rGO/ZnMn2O4@PPy were deformed. This was mainly related to the increasing ionic transfer resistance due to the limit diffusion.[26,38,39] **Figure 5-a** exhibit the CV spectra of rGO/$ZnMn_2O_4$ and rGO/ $ZnMn_2O_4$@PPy at the 5-mV/s scan rate, and the spectra of both samples are rectangular. As shown in **Fig. 5a**, the CV curve of rGO/$ZnMn_2O_4$@PPy had a larger integrated area compared to the CV curve of rGO/$ZnMn_2O_4$. The CV spectra showed that electrodes made of rGO/$ZnMn_2O_4$ and rGO/ $ZnMn_2O_4$@PPy had similar electrochemical behavior, but the specific capacitance of rGO/ $ZnMn_2O_4$@PPy was higher than the specific capacitance of rGO/$ZnMn_2O_4$. The presence of the PPy in the hybrid aerogel improved the electrical conductivity of the materials and ensured the rapid charge transportation.[40] The CVs of rGO/$ZnMn_2O_4$@PPy showed the similar rectangular shape of the curves when changing the scan rate from 5 mV/s to 100 mV/s. Thus, rGO/$ZnMn_2O_4$@PPy could work at high voltage/current charge/discharge rates due to good ionic conductivity.[40]

Galvanostatic Charge-Discharge Studies

The power density and specific capacitance of the hybrid aerogel electrodes were investigated by the chronopotentiometry technique. Figure 6 displays the charge-discharge curves of the aerogel materials in two aqueous electrolytes, 1 M H_2SO_4 and 1 M Na_2SO_4. The measurements were carried out with varying the current density in the range from 0.2 A/ g to 5 A/g and varying the potential over time. The specific capacitance value was calculated as follows:

$$C_s = \frac{I \cdot \Delta t}{m \cdot \Delta V} \qquad (3)$$

where *I* denotes the applied current (A), At is the time taken for the discharge, m is the mass of active electrode material, and AV is the discharge potential.

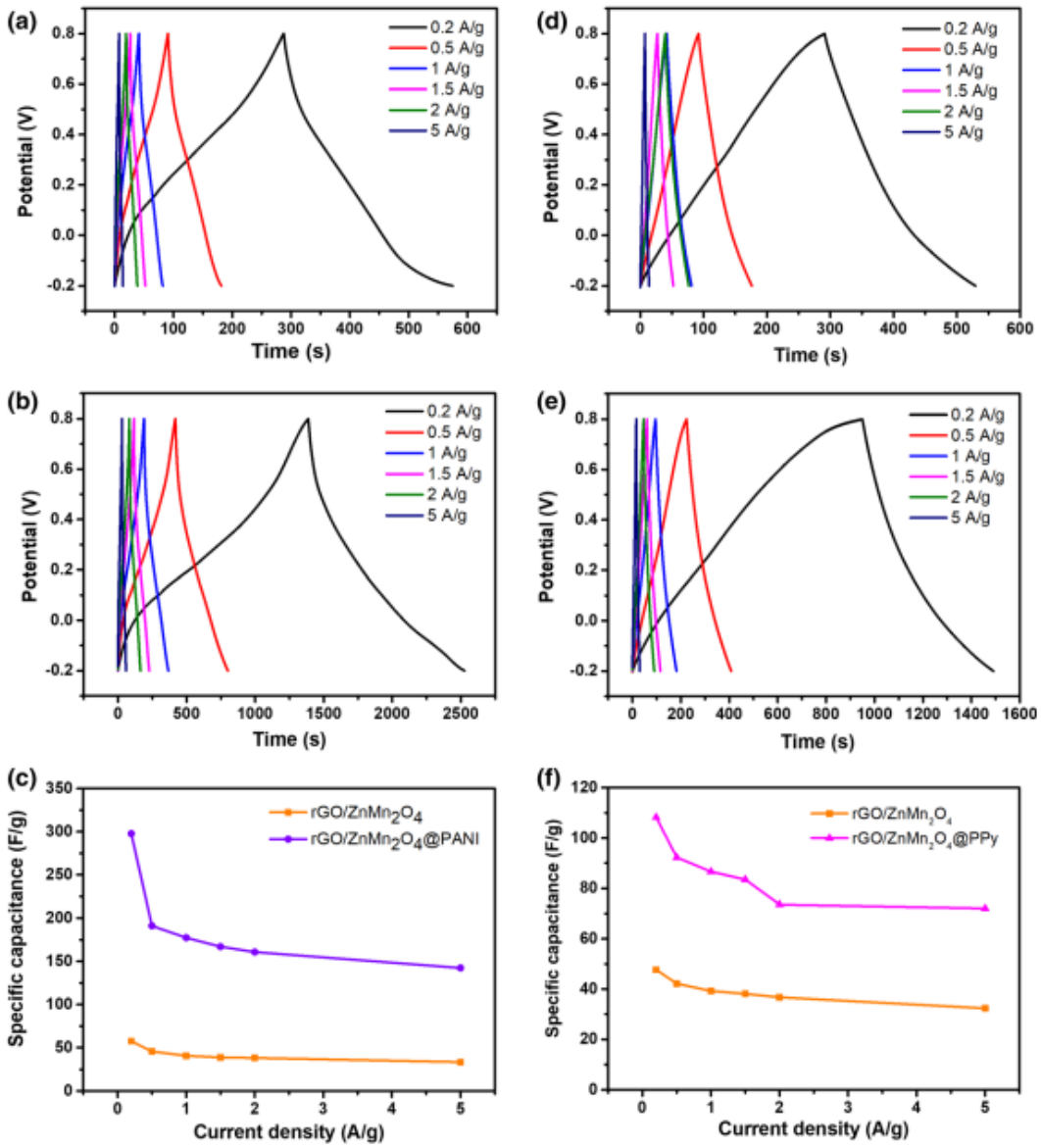

Fig. 6. Charge-discharge plots in 1 M H_2SO_4 of (a) rGO/$ZnMn_2O_4$, (b) rGO/$ZnMn_2O_4$@PANI, and (c) their specific capacitance calculated from galvanostatic curves. Charge-discharge plots in 1 M Na_2SO_4 of (d) rGO/$ZnMn_2O_4$, (e) rGO/$ZnMn_2O_4$@PPy, and (f) their specific capacitance calculated from galvanostatic curves.

Figure 6a and b shows the charge-discharge curves of rGO/$ZnMn_2O_4$ and rGO/$ZnMn_2O_4$@PANI tested in an H_2SO_4 electrolyte at various current densities. It can be seen that rGO/$ZnMn_2O_4$@PANI exhibited a longer drop rate than rGO/$ZnMn_2O_4$. Accordingly, a longer time on the discharge curve for rGO/$ZnMn_2O_4$@PANI corresponds to a higher specific capacitance compared with the others. The specific capacitance of rGO/$ZnMn_2O_4$@PANI at a current density of 0.2 A/g is 297.8 F/g, whereas for rGO/$ZnMn_2O_4$ it is only 57.5 F/g in the same conditions. **Figure 6a** and b shows the ideal triangular symmetric charge-discharge curve displaying the good reversibility and fast redox activity of both samples in the H_2SO_4 electrolyte. When the current density decreased, the Cs values increased. This phenomenon may stem from the limited ionic kinetics for the discharging process. A lower current

density supported electrolyte ions penetrating through the surface into the inner layer of the electrode materials. This could improve the inser-tion/exertion process leading to higher specific capacitance and pseudocapacitive behavior.

Therefore, the charge-discharge process for rGO/ $ZnMn_2O_4$ and rGO/$ZnMn_2O_4$@PPy in Na_2SO_4 was studied at various current densities in the range 0.2-5 A/g (**Fig. 6d and e**). In the current density scan of 0.2 A/g, the slightly non-linear discharge curves of both samples exhibited an IR drop, which indicates the presence of internal resistance and Faradic materials.[41] The discharge time increased in the PPy-loaded samples illustrating its positive effect. PPy is known as a pseudo-capacitive material.[42] When it was applied to the rGO/$ZnMn_2O_4$, it yielded a nearly symmetrical plot and increased the surface area with the redox-active. With the addition of PPy, the charge-discharge time increased, which means that the specific capacitance had increased. The specific capacitance of rGO/ $ZnMn_2O_4$@PPy recorded at 0.2 A/g was 108.24 F/g, which is two times higher compared to GA/ $ZnMn_2O_4$ recorded in the same conditions. The specific capacity calculated from the galvanostatic curves for 1 M H_2SO_4 and 1 M Na_2SO_4 is shown in **Fig. 6c** and f, respectively. Consequently, the specific capacitance of aerogels decreases with the increase of the current densities scan rate, which could be attributed to the slowdown of electrolyte ions diffusion into the electrode materials.

Electrochemical Impedance Studies

A Nyquist plot was recorded in the frequency range from 0.01 Hz to 100 kHz, where the imaginary part Z'' is plotted against the real part *Z'* **(Fig. 7).** A semicircular region, which can be attributed to low charge transfer resistance or high conductivity of the sample, was detected in the high-frequency region of the spectra. This part represented the equivalent series resistance (ESR) and charge transfer resistance (R_{ct}) of the electrodes. The next part of the plot exhibited an inclined line in a low-frequency region. This part can be attributed to the Warburg impedance or diffusive resistance between the electrode aerogel materials and the electrolyte ions. The almost linear vertical line across the *Z'* part of the higher rezistivity region implies a nearly ideal capacitive behavior for the materials, and the steeper-sloped line shows the fast diffusion of the electrolyte to the electrode

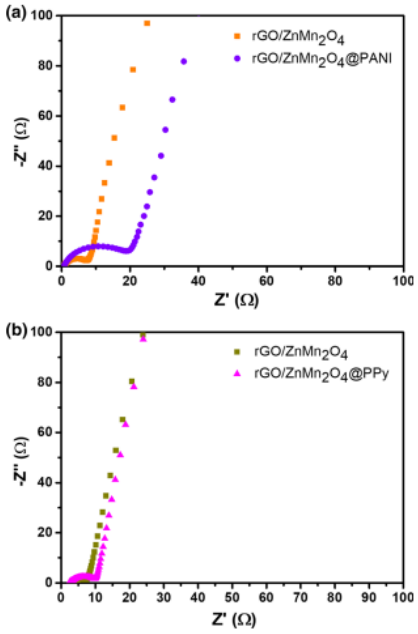

Fig. 7. Electrical impedance spectra of the hybrid aerogel structures of (a) rGO/$ZnMn_2O_4$, rGO/$ZnMn_2O_4$@PANI tested in 1 M H_2SO_4, and (b) rGO/$ZnMn_2O_4$, rGO/$ZnMn_2O_4$@PPPy tested in 1 M Na_2SO_4.

The ESR values were taken at the first interception point with the *Z*′ axis and consisted of total resistance from the electrolyte and electrode.[41,43] In particular, R_{ct} represents the charge transfer rate at the electrode and electrolyte interface, which could further bring on the Faradaic redox process.[44] Rct can be determined from the diameter of the semicircle formed. **Figure 7a** shows the EIS plot of rGO/$ZnMn^2O^4$ and rGO/$ZnMn^2O^4$@PANI in 1 M H^2SO^4, the acquired values of the materials R_{ct} being 6.4 Ω and 18.06 Ω, respectively. Compared to the R_{ct} of rGO/$ZnMn^2O^4$ and rGO/$ZnMn^2O^4$@PPy studied in 1 M Na^2SO^4, the acquired values, as shown in **Fig. 7b**, display lower resistance, which were 3.51 Ω and 6.92 Ω, respectively. Higher R_{ct} values are due to the higher serial interfacial resistance and a Faradaic reaction that involves the exchange of ions between the electrolyte and the electrode.[45] Consequently, in the same conditions, the hybrid aerogel structures modified with conductive polymers have lower ESR values compared to rGO/$ZnMn_2O_4$.

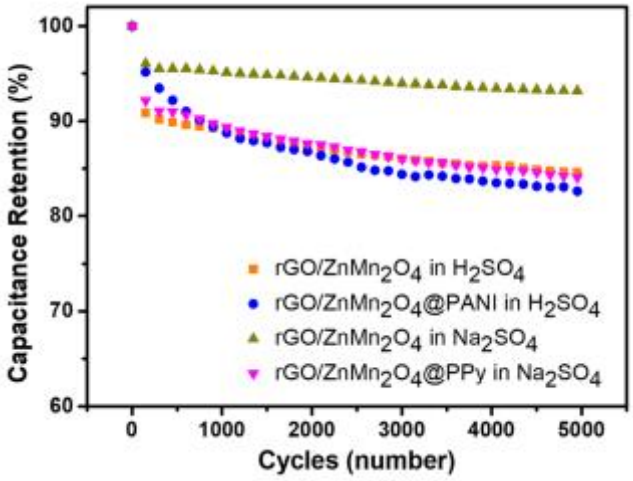

Fig. 8. Cyclic capacity retention during 5000 cycles at 0.2 A/g.

The ESR values of rGO/$ZnMn_2O_4$@-PANI (0.82 Ω) and rGO/$ZnMn_2O_4$@PPy (2.86 Ω) are higher than those of the rGO/$ZnMn_2O_4$ in 1 M H2SO4 (0.87 Ω) and in 1 M Na_2SO_4 (3.34Ω), due to an increase of conductivity as a result of the PANI and PPy, respectively.

Cyclic Stability

Cycling performance is essential for the practical application of SCs. In this study, the cycling stabilities of rGO/$ZnMn_2O_4$, rGO/$ZnMn_2O_4$@PANI, and rGO/$ZnMn_2O_4$@PPy electrodes were measured at a current density of 0.2 A/g for 5000 cycles in a two-electrode symmetrical SC. The specific capacitance retention of the electrodes is shown in **Fig. 8**. In contrast to rGO/$ZnMn_2O_4$ electrodes measured in Na_2SO_4, the other samples' specific capacitances gradually decreased with the increase of cycle numbers in both conditions of the H_2SO_4 electrolyte and the Na_2SO_4 electrolyte. It has been reported that supercapacitor electrodes made of both PANI[46] and PPy[47] showed poor capacitance retention due to their mechanical degradation by the significant volumetric change in the doping/dedoping process and low rate capability. This led to poor cycling stability through the charge-discharge processes over long periods of both PANI and PPy. In the presence of $ZnMn_2O_4$ in the electrodes, after a continuous

5000 cycles of charge-discharge, the materials exhibited a high cycling stability of the supercapacitor. The rise in capacitance retention might be due to the activation of the surface, leading to a better pathway of electrolyte ions to the active sites of smaller mesopores when $ZnMn_2O_4$ was used as the spacer. The capacitance retentions of rGO/ $ZnMn_2O_4$ and rGO/$ZnMn_2O_4$@PANI in H_2SO_4 were 84.58% and 82.47%, respectively. When the samples were tested using Na_2SO_4 as the electrolyte, the retentions of rGO/$ZnMn_2O_4$ and rGO/ $ZnMn_2O_4$@PPy were 93.27% and 84.03%,respectively.

CONCLUSIONS

Three-dimensional hybrid aerogel materials based on rGO and $ZnMn_2O_4$ were prepared by a one-step hydrothermal co-assembly method. The hybrid aerogels were then modified by PANI and PPy using the in situ polymerization method. The resulting materials have a high porosity nanoarchitecture, and demonstrate the properties of both pseudo-capacitive and electric double-layer capacitive materials, which provide improved capacitive behavior and increased cyclic stability of SCs in aqueous electrolytes. The obtained results show that PANI and PPy promote charge transfer and significantly improve the specific supercapacitance of the aerogel-based electrode materials.

REFERENCES

1. B. Luo, D. Ye, and L. Wang, Adv. Sci. 4, 1 (2017).

2. D.P. Dubal, N.R. Chodankar, D.H. Kim, and P. Gomez-Ro-mero, Chem. Soc. Rev. 47, 2065 (2018).

3. Z. Li, S. Gadipelli, Y. Yang, G. He, J. Guo, J. Li, Y. Lu, C.A. Howard, D.J.L. Brett, I.P. Parkin, F. Li, and Z. Guo, Energy Storage Mater. 17, 12 (2019).

4. M.F. Iqbal, M.N. Ashiq, A. Razaq, M. Saleem, B. Parveen, and M. Hassan, Electrochim. Acta 273, 136 (2018).

5. M.P. Down, S.J. Rowley-Neale, G.C. Smith, and C.E. Banks, ACS Appl. Energy Mater. 1, 707 (2018).

6. V.C. Tran, S. Sahoo, J. Hwang, V.Q. Nguyen, and J.J. Shim, J. Electroanal. Chem. 810, 154 (2018).

7. Z. Niu, L. Liu, L. Zhang, Q. Shao, W. Zhou, X. Chen, and S. Xie, Adv. Mater. 26, 3681 (2014).

8. S. Yang, Z. Han, J. Sun, X. Yang, X. Hu, C. Li, and B. Cao, Electrochim. Acta 268, 20 (2018).

9. J.A. Rajesh, B.K. Min, J.H. Kim, H. Kim, and K.S. Ahn, J. Electrochem. Soc. 163, A2418 (2016).

10. V. Shanmugavalli and K. Vishista, Mater. Res. Express 6, 045021 (2019).

11. Y. Wang, J. Guo, T. Wang, J. Shao, D. Wang, and Y.W. Yang, Nanomaterials 5, 1667 (2015).

12. S.K. Chang, Z. Zainal, K.B. Tan, N.A. Yusof, W.M.D.W. Yusoff, and S.R.S. Prabaharan, Ceram. Int. 41, 1 (2015).

13. J. Ma, H. Fan, X. Zheng, H. Wang, N. Zhao, M. Zhang, A.K. Yadav, W. Wang, W. Dong, and S. Wang, J. Hazard. Mater. 387, 122017 (2020).

14. N. Zhao, H. Fan, M. Zhang, J. Ma, Z. Du, and B. Yan, Chem. Eng. J. 390, 124477 (2020).

15. M. Zhang, Y. Xu, H. Fan, N. Zhao, B. Yan, C. Wang, J. Ma, A.K. Yadav, W. Zhang, Z. Du, X. Zheng, M. Li, G. Dong, and W. Wang, J. Alloys Compd. 826, 154115 (2020).

16. N. Zhao, H. Fan, M. Zhang, J. Ma, C. Wang, A.K. Yadav, H. Li, X. Jiang, and X. Cao, Nano Energy 71, 104626 (2020).

17. M.Q. Menaka, S.E. Lofland, K.V. Ramanujachary, and A.K. Ganguli, Bull. Mater. Sci. 32, 231 (2009).

18. M. Abdollahifar, S.S. Huang, Y.H. Lin, Y.C. Lin, B.Y. Shih, H.S. Sheu, Y.F. Liao, and N.L. Wu, J. Power Sour. 378, 90 (2018).

19. P.E. Saranya and S. Selladurai, J. Mater. Sci.: Mater. Electron. 29, 3326 (2018).

20. K. Naoi, W. Naoi, S. Aoyagi, J.I. Miyamoto, and T. Kamino, Acc. Chem. Res. 46, 1075 (2013).

21. N.A. Kumar, H.J. Choi, Y.R. Shin, D.W. Chang, L. Dai, and J.B. Baek, ACS Nano 6, 1715 (2012).

22. A. Bahloul, B. Nessark, E. Briot, H. Groult, A. Mauger, K. Zaghib, and C.M. Julien, J. Power Sour. 240, 267 (2013).

23. A. Ladron-de-Guevara, A. Bosca, J. Pedros, E. Climent-Pascual, A. de Andres, F. Calle, and J. Martinez, Appl. Surf. Sci. 467-468, 691 (2019).

24. H. Zhou, Z. Yan, X. Yang, J. Lv, L. Kang, and Z.H. Liu, Mater. Chem. Phys. 177, 40 (2016).

25. G. Wang, L. Jin, J. Ye, and X. Li, Mater. Chem. Phys. 122, 224 (2010).

26. P.A. Basnayaka, M.K. Ram, L. Stefanakos, and A. Kumar, Graphene 02, 81 (2013).

27. Q. Cheng, J. Tang, J. Ma, H. Zhang, N. Shinya, and L.C. Qin, J. Phys. Chem. C 115, 23584 (2011).

28. K. Zhang, L.L. Zhang, X.S. Zhao, and J. Wu, Chem. Mater. 22,1392 (2010).

29. P. Sekar, B. Anothumakkool, and S. Kurungot, ACS Appl. Mater. Interfaces 7, 7661 (2015).

30. H. Xu, H. Jiang, X. Li, and G. Wang, RSC Adv. 5, 76116 (2015).

31. H. Fei, N. Saha, N. Kazantseva, T. Babkova, M. Machovsky, G. Wang, H. Bao, and P. Saha, J. Mater. Sci.: Mater. Electron. 29, 3025 (2018).

32. Y.M. Cai, Z.Y. Qin, and L. Chen, Prog. Nat. Sci. Mater. Int. 21, 460 (2011).

33. T. Huang, C. Zhao, Z. Qiu, J. Luo, and Z. Hu, Ionics (Kiel) 23, 139 (2017).

34. Y. Liu, J. Bai, X. Ma, J. Li, and S. Xiong, J. Mater. Chem. A 2, 14236 (2014).

35. X. Li, H. Song, Y. Zhang, H. Wang, K. Du, H. Li, Y. Yuan, and J. Huang, Int. J. Electrochem. Sci. 7, 5163 (2012).

36.Y.G. Wang, H.Q. Li, and Y.Y. Xia, Adv. Mater. 18, 2619 (2006).

37. J. Yan, T. Wei, B. Shao, Z. Fan, W. Qian, M. Zhang, and F. Wei, Carbon N. Y. 48, 487 (2010).

38. C. Wang, Y. Zhan, L. Wu, Y. Li, and J. Liu, Nanotechnology 25, 305401 (2014).

39. S. Ardizzone, G. Fregonara, and S. Trasatti, Electrochim. Acta 35, 263 (1990).

40. H. Zhuo, Y. Hu, Z. Chen, and L. Zhong, Carbohydr. Polym. 215, 322 (2019).

41. M.D. Stoller and R.S. Ruoff, Energy Environ. Sci. 3, 1294 (2010).

42. G.A. Snook, P. Kao, and A.S. Best, J. Power Sour. 196, 1 (2011).

43. Y.S. Lim, Y.P. Tan, H.N. Lim, N.M. Huang, and W.T. Tan, J. Polym. Res. 20, 156 (2013).

44. H. Du, Y. Xie, C. Xia, W. Wang, and F. Tian, New J. Chem. 38, 1284 (2014).

45. H.P. Cong, X.C. Ren, P. Wang, and S.H. Yu, Energy Environ. Sci. 6, 1185 (2013).

46. L. Li, A.R.O. Raji, H. Fei, Y. Yang, E.L.G. Samuel, and J.M. Tour, ACS Appl. Mater. Interfaces 5, 6622 (2013).

47. H. Zhu, M. Li, D. Wang, S. Zhou, and C. Peng, J. Elec-trochem. Soc. 164, A1820 (2017).